On the calibration of the specific barrier model to the NGA dataset

K.M. Foster
Virginia Tech, Blacksburg VA, USA

B. Halldorsson
Earthquake Engineering Research Centre, University of Iceland, Selfoss, Iceland

R.A. Green, & M.C. Chapman
Virginia Tech, Blacksburg VA, USA

SUMMARY:
The specific barrier model is a self-consistent and physically based earthquake source model. Its far-field source spectrum can be established based on a few primary model parameters. It has recently been calibrated to the NGA dataset of earthquake strong motions by Foster et al. (2012). In this paper we investigate further the model calibration and interpret the results in terms of the seismological model applied. We control the trade-off between the local stress drop and κ, and conclude a κ-filter is required for describing the high-frequency diminution of diverse strong-motion datasets. We investigate how our predictions of pseudo-spectral acceleration normalized by peak-ground acceleration (PSA/PGA), and that of an empirical model, tend not to fit the NGA data at long distances (≥150 km). No path model applied resolved this misfit. We discuss how the strong-motion characteristics of the Chi-Chi earthquakes may be incompatible with the rest of the NGA dataset.

Keywords: strong-motion, local stress drop, kappa

1. INTRODUCTION

Empirical ground motion prediction equations are useful for quantifying the relationship of the spectral amplitudes of the parameters of interest to earthquake engineers (e.g., peak ground motion, peak structural response parameters) with distance and frequency. Seismic design of structures may however require simulation of the time histories of the expected earthquake strong ground motions at a given site due to an earthquake of a given magnitude. This necessitates a more ‘physical’ approach and in the past the stochastic method has been widely used (Boore 1983, 2003). The method is based on a seismological model that contains a simplified spectral description of the waves radiating from the earthquake source, along with spectral filters quantifying the effects of propagation path and site conditions on observed ground motion. While models exist that account for both P and S waves, along with reflected phases and surface waves, the application of the stochastic method generally focuses solely on the S wave train, because it is most responsible for earthquake damage.

The specific barrier model (SBM) is an earthquake source model that is particularly useful for simulation of earthquake strong-motion over the entire frequency and distance ranges of engineering interest (Papageorgiou & Aki 1983a; b). The salient features of the SBM making it suitable for this purpose are: (1) the SBM contains a self-consistent and physically meaningful description of the faulting process of a finite-size, composite seismic source i.e., an earthquake source composed of smaller sub-sources (subevents) (Figure 1.1a); (2) it is fully characterized by only five parameters; (3) the spectral expression of the radiated S waves in the far-field region (far-field source spectrum) (Figure 1.1b) exists in closed form making it especially suitable for application in the stochastic method. It has been shown that the SBM captures the main features of more complex composite earthquake sources. Additionally, it has been applied in the simulation of earthquake strong-motion time histories, and structural response, both in the near-fault and far-field region of earthquakes (see e.g., Papageorgiou & Aki 1985; Papageorgiou 1988, 2003; Halldorsson & Papageorgiou 2005; Halldorsson, Ólafsson, & Sigbjörnsson 2007; Halldorsson, Mavroeidis, & Papageorgiou 2011; Foster *et al.* 2012; Halldorsson & Papageorgiou 2012a, b and references therein)

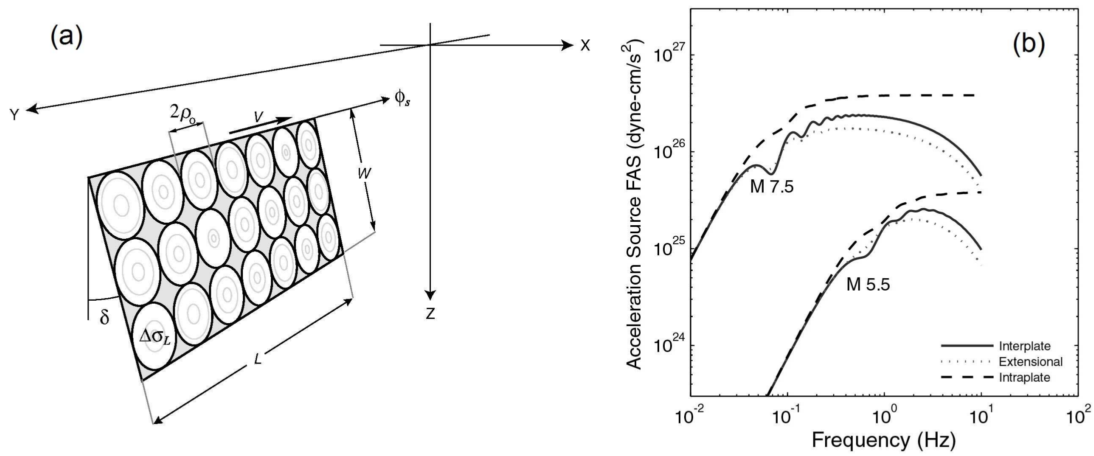

Figure 1.1. (a) A schematic view of the SBM representing the earthquake fault consisting of equal-size subevents arranged in a non-overlapping manner on the fault plane. Subevent rupture starts at the center of each crack associated with a 'local stress drop' $\Delta\sigma_L$ and spreads radially outwards (the rupture fronts at successive time instants are denoted by the light circles) until it is arrested by the barriers, denoted by the shaded area between the cracks. (b) The specific barrier model source spectra for three different tectonic regions. The interplate and extensional source spectra are non-self similar and affected by high-frequency diminution i.e., $S(f, M_\circ, \zeta) \cdot D(f, \kappa)$ ($\log \zeta = 2s_m(M_w - 6.35)$, $s_m = -0.12$, and $\kappa = 0.05$ s; see Table 8 in HP05). The spectra are shown for M_w5.5, and 7.5 as calibrated by Halldorsson and Papageorgiou (2005) (from Fea12).

The previous calibration of the SBM to earthquake motions from different tectonic regions in the context of the stochastic method and random vibration theory (Halldorsson & Papageorgiou 2005; denoted by HP05) has been updated using the much larger, "unified" NGA database of strong-motions from interplate earthquakes of shallow crustal regions (Foster *et al.* 2012; Fea12 hereafter). The seismological model of Fea12 fits the NGA subsets quite well using nearly the same model parameters as HP05, but also differs in important aspects. In this paper we review and expand on the results of Fea12. We present our results using the methodology developed by Spudich *et al.* (1999) to represent the fit of a seismological model to a dataset, and a novel method based on the ratio of pseudo-spectral acceleration (PSA) to peak-ground acceleration (PGA). We show that analyses of model residuals can highlight important aspects of the fit of a seismological model to a dataset. In a physically based seismological model, such analyses can provide clues to the origin of the discrepancy in terms of physical parameters. We show how the recently calibrated seismological model tends to underpredict the spectral response amplitudes of earthquake ground motions at long distances (≥150 km). We investigate the source of this discrepancy using a number of independently obtained path attenuation functions in the seismological model and compare the predictions of our model with empirical relationships using largely the same data. Additionally, we show that a kappa-filter effectively describes diminution of high-frequency spectral amplitudes for datasets with records from different earthquakes and stations. We discuss the characteristics of the PSA/PGA spectrum, whose shape is sensitive to changes in κ (high-frequency diminution parameter) but not $\Delta\sigma_L$ (controlling parameter of the SBM), and use it to compare our model predictions with NGA data. The behaviour of the curves supports our observation that κ and $\Delta\sigma_L$ affect frequency-dependent residual behaviour in a fundamentally different manner across the frequency range of calibration, largely eliminating the issue of parameter tradeoffs. Finally, we show how the strong-motion characteristics of the Chi-Chi data may be different from the rest of the NGA dataset.

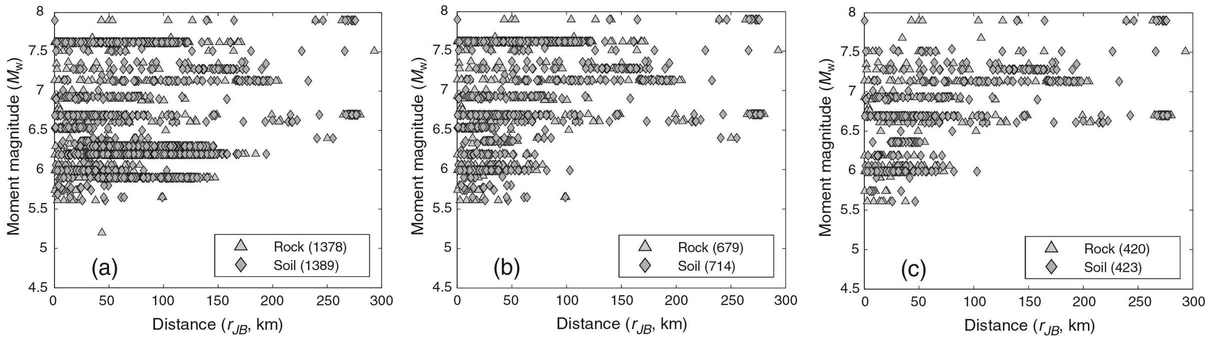

Figure 2.1. Magnitude-distance plots of the three datasets used in this study. (a): Complete NGA dataset; (b): NGA dataset excluding Chi-Chi aftershock data; (c): Same as (b), except excluding earthquakes associated with active tectonic extension (Spudich et al., 1999), and the Chi-Chi mainshock data.

2. CALIBRATION OVERVIEW

Since Papageorgiou & Aki (1983a; b) developed and introduced the SBM, several studies have been published improving its usability for engineering applications. The developments are briefly summarized below:

- Establishment of the scaling law for the SBM based on observed model parameters (Papageorgiou & Aki 1985; Aki & Papageorgiou 1988).
- The presentation of a closed-form equation for the aggregate far-field source spectrum from the SBM (see Figure 1.1b) (Papageorgiou 1988) on the basis of the formulation for a composite earthquake source composed of multiple identical subevents (Joyner & Boore 1986).
- Calibration of the SBM to shallow crustal earthquakes of three different tectonic regions, using a seismological model combining the SBM source spectrum derived by Papageorgiou (1988) with suitable regional path and site terms drawn from the literature (Halldorsson & Papageorgiou 2005).
- A theoretical study of the sensitivity of the far-field source spectrum to variations to the fundamental assumptions in the SBM, allowing for variable size-subevents and accounting for different isochrone distributions (Halldorsson & Papageorgiou 2012a; b). The results indicate that in the absence of physical information on the selection of subevent-size distribution, the SBM appears to be the most parsimonious, yet effective, way to capture the essential characteristics of a composite seismic source
- Calibration of the SBM to a larger and unified dataset of strong-motions from shallow crustal earthquakes in interplate regions (Fea12). This study considerably expanded on the HP05 study by performing a calibration (analogously to HP05) using the full NGA dataset (Chiou *et al.* 2008; Power *et al.* 2008) and both soil and rock data (HP05 only used data recorded on soil).

While the seismological model and calibration procedure were similar in HP05 and Fea12, we focus here on the distinguishing aspects of the latter calibration and the insights gained from it. For brevity's sake we also omit detailed discussion of the functional form of the SBM far-field source spectrum in this paper. For a concise summary of the calibration and its results we refer the reader to Fea12.

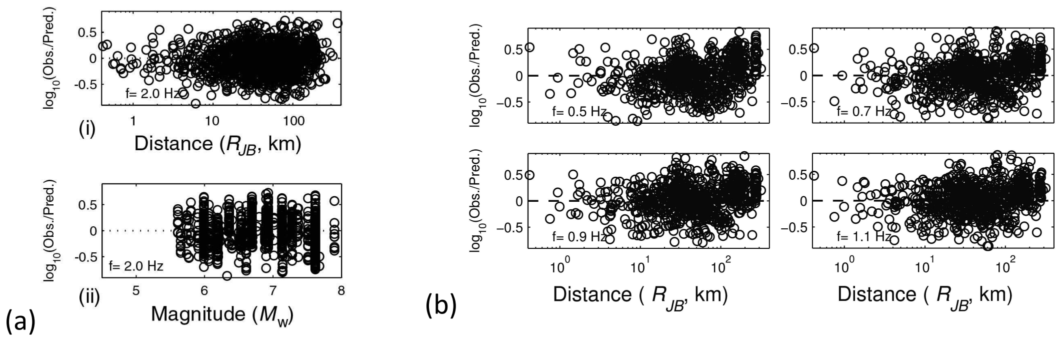

Figure 2.2. (a) Residuals of the seismological model's prediction of spectral ordinates at $f = 2$ Hz for dataset (c) plotted vs. (i) log-distance and (ii) moment magnitude. The residual clouds appear balanced on the zero line (i.e., zero bias) and do not exhibit any apparent (or quantified) trends with increasing distance nor magnitude. (b) Residuals of four separate bins at $f = 0.5$-1.1 Hz plotted vs. log-distance showing distance dependent behavior, manifested by a positive slope of a least-squares line fitted to the residuals.

For completeness however, we revisit the functional form of the seismological model in Fea12 and HP05 (Boore 1983, 2003):

$$Y(f, M_\circ, r) = E(f, M_\circ) \cdot P(f, r) \cdot G(f) \cdot I(f) \tag{2.1}$$

where: f is frequency; the $E(f, M_\circ)$, $P(f, r)$, and $G(f)$ terms account for source,path,and site effects,respectively; and $I(f)$ is the "instrumental term" for providing the 5% damped PSV used in this study. The model was applied using the stochastic method in combination with random vibration theory (RVT) to generate predictions of the most likely PSV ordinates at a range of discrete spectral periods (Boore 1983, 2003). In Fea12 we used three subsets of the NGA dataset (Figure 2.1) to calibrate the seismological model. We proceeded by generating estimates of PSV for each observation in the database and plotting residual clouds against magnitude and distance (see e.g., Figure 2.2a), divided into twelve log-spaced frequency bins from 0.5 to 10 Hz.

In Equation (1), the source term is $E(f, M_\circ) \sim S(f, M_\circ, \zeta) \cdot D(f, \kappa)$ where $D(f, \kappa)$ is the high frequency diminution term (HFD) and $S(f, M_\circ, \zeta)$ is the far-field spectrum of the earthquake source, modeled by the SBM. HP05 compared the effects of modeling high-frequency diminution with different filtering functions. HFD in observed ground motion has been attributed to both source (Aki & Papageorgiou, 1988) and site (e.g., Hanks, 1982; Anderson & Hough, 1984) effects. But, in our

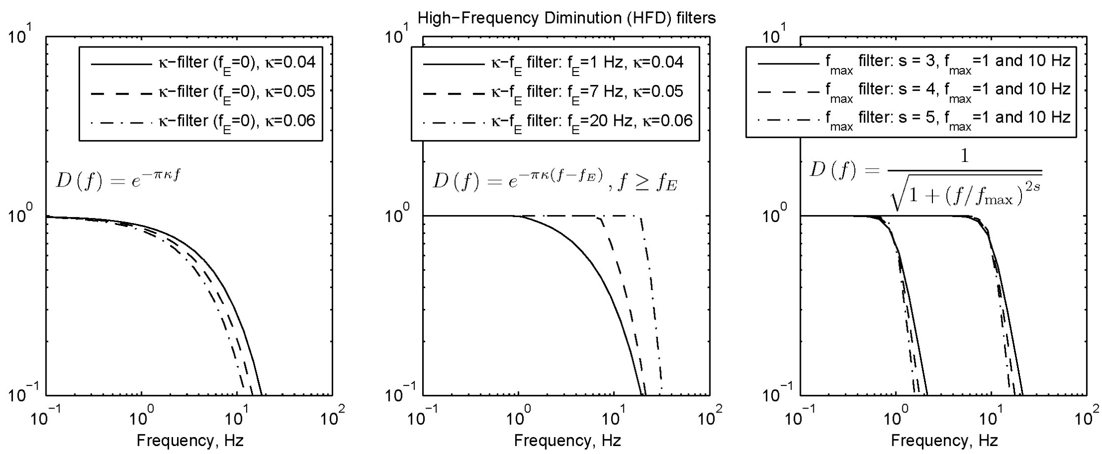

Figure 2.3. High-frequency diminution (HFD) filters commonly employed in seismological models. Left: "kappa" filter with f_E=0 and several values of κ. Middle: "kappa" filter with several (nonzero) values of f_E and κ. Right: f_{max} filter with several values of s and f_{max}.

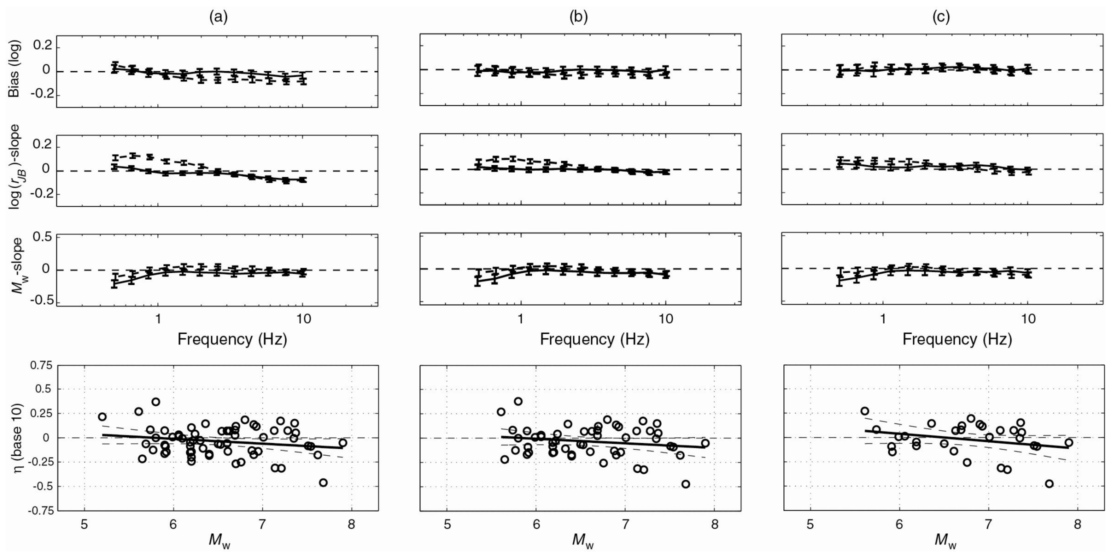

Figure 2.4. The fit of a seismological model to the three datasets in Figure 2.1, expressed in terms of residual behaviour using the method of Spudich et al. (2009). For each dataset (a)-(c) (left to right), respectively, each of the following is shown: mean bias (top), log-distance dependence (upper middle), and magnitude dependence (lower middle) of the residuals between the dataset and the seismological model applied. Solid and dashed lines denote residual behaviour associated with rock and soil sites, respectively. Error bars show +/-1 standard deviation of the respective maximum-likelihood estimates. The top vertical scale shows base-ten logarithms of the residuals. The bottom plot shows inter-event residuals (η_i) as a function of magnitude. The solid and dashed lines are the least-squares regression line and its 95% confidence limits.

model we apply the HFD filter solely to the source term. In doing so, we are implicitly assuming one of two possibilities: (a) HFD is a universal characteristic of ground motion regardless of the point of observation. Therefore site characteristics are irrelevant, *i.e.* the HFD is attributed solely to the source. (b) HFD is a characteristic of both source and site. HFD will vary in the degree of influence based on site properties. We take the pragmatic latter stance here, acknowledging the influence of both source and site HFD mechanisms and attempting to describe the NGA data by a single HFD function without separating the relative site and source contributions quantitatively.

Figure 2.3 presents the most common filtering functions, the so-called κ and $f_{\max}$ functions. In large ground motion datasets, both onset frequency (*i.e.*, f_E and $f_{\max}$ in Figure 2.3) and rates of decay (*i.e.*, κ and s) will vary substantially among individual recordings and thus "smear out" when the data are taken as a whole (Trifunac 1994). As HP05 concluded, we found in our calibrations that a κ-filter with zero onset frequency results in the best fit of the seismological model to the high-frequency spectral data of the NGA dataset. We suggest that the "smooth" shape of a κ-filter with $f_E=0$ works well because it best accounts for the variation of HFD among individual records in a large dataset.

In our calibration, local stress drop or $\Delta\sigma_L$ and κ were the two independent variables of most interest. $\Delta\sigma_L$ and κ affect the source spectral amplitudes to a different extent, and in fundamentally different way, at different frequencies. $\Delta\sigma_L$ controls the high-frequency source spectral levels, which are flat above the second corner frequency (e.g., the intraplate spectra in Figure 1.1b) whereas κ's increasing diminution with frequency stems from the filter shape in Figure 2.3 (Figure 5 in Fea12 demonstrates this behavior in terms of mean residual bias). Because of the different manner in which $\Delta\sigma_L$ and κ affect the source spectrum, Fea12 controlled the extent of trade-off between $\Delta\sigma_L$ and κ and found their combination that results in zero model bias over the frequency range considered.

Brillinger & Preisler (1984, 1985) and Strasser, Abrahamson, & Bommer (2009) discuss the necessity of accounting for imbalance in strong-motion datasets. Both HP05 and Fea12 applied the random effects model by Abrahamson & Youngs (1992) and split each residual into two components, an

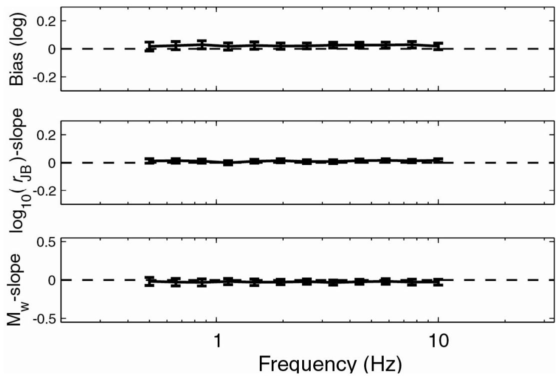

Figure 3.1. The fit of Boore & Atkinson's (2008) empirical GMPE predictions to the NGA dataset. The subset used is BA08's, and 1,249 records remained after applying our exclusion criteria. No distinction is made between soil and rock residuals here, since V_{s30} data were input to BA08 directly from the NGA data

"inter-event" and an "intra-event" component, in order to account for the imbalanced datasets. Following the calculation of inter- and intra-event residuals, we used the maximum-likelihood (ML) formalism of Spudich *et al.* (1999) to concisely represent the performance of the model. Figure 2.4 presents our results using Sea99's formalism showing mean residual bias, as well as the distance-dependence and magnitude-dependence for various frequency bins. Distance- and magnitude-dependency are quantified by the slopes of least-squares lines fit to the residuals in each bin (see Figure 2.2). We expect low overall model bias at all or most frequencies for a model that performs well. We suggest that inter-event residuals (Figure 2.4, bottom) that are high or low, relative to the database average, may act as a proxy for the events' stress drops being higher or lower than average.

3. COMPARISON WITH EMPIRICAL GMPES

A seismological model of the type shown in Equation (1) where the underlying functional forms are based on theory and have few parameters will have a poorer fit to a given dataset than many empirical ground motion prediction equations (GMPEs), which often have a greater number of independent parameters that additionally can take different values at each discrete frequency. We exemplify this by showing in Figure 3.1 the overall mean residual bias, distance dependence and magnitude dependence of the residuals for the empirical relation by Boore & Atkinson's (2008; BA08 hereafter) vs. the NGA dataset. As expected, the flexible BA08 relation fits the data well. One significant distinction between the fits shown in Figure 3.1 and Figure 2.4 is worth noting. In evaluating our SBM seismological model predictions, NGA sites were categorized in a binary fashion, on the basis of the effective shear wave velocity of the uppermost 30 meters of the lithosphere beneath the site, V_{s30}. One of two site amplification functions (soil, for V_{s30} < 360 m/s, or rock otherwise) was then used to generate model predictions, regardless of the V_{s30} datum in the NGA flatfile. By contrast, when generating the plot in Figure 3.1, the V_{s30} values from the NGA flatfile were provided as inputs to the BA08 GMPE.

4. THE PSA/PGA METHOD AND VARIOUS PATH MODELS

Our best-fit value of $\kappa = 0.06$ s differs from the HP05 calibration (which found $\kappa = 0.05$ s). We evaluated this result in a different way by examining the pseudospectral accelerations normalized by peak ground acceleration (PSA/PGA). We binned the NGA data of subset (c) into magnitude- and distance-bins, and compared the PSA/PGA ratios for these bins to the corresponding predictions from the seismological model. Figure 4.1 shows an example of the comparison for earthquakes of $M_w 6-7$ and at six distance bins with lower distance limits of $r_{JB} = 0$, 10, 20, 40, 80, and 150 km. The PSA/PGA ratios for each record are plotted with gray lines. The thin black solid lines denote their average value for each bin, and the thin dashed black lines correspond to +/- 1 standard deviation. The thick solid lines denote the predictions from the seismological model for $\Delta\sigma_L = 160$ bar and $\kappa =$

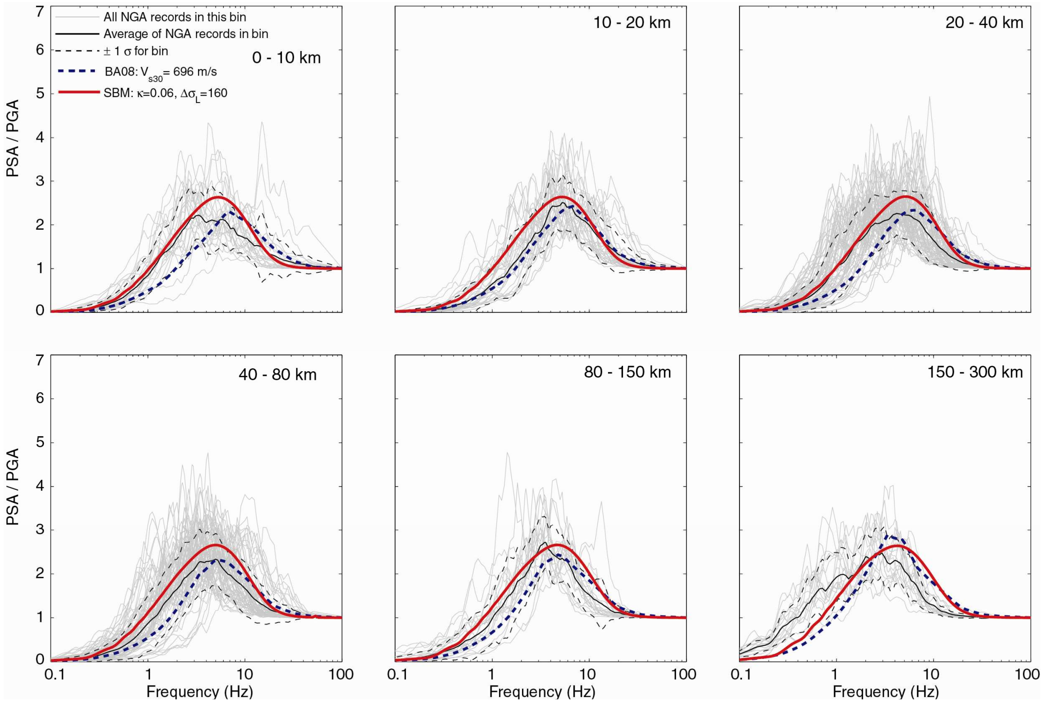

Figure 4.1. The PSA/PGA ratio on rock (gray curves) of earthquakes of M_w6-7 in dataset (c), plotted as a function of frequency for six separate distance bins: 0-10, 10-20, and 20-40 km (top left to right) and 40-80, 80-150 and 150-300 km (bottom left to right), respectively. The average ratio for each distance bin is denoted by the thin black curve and its +/- one standard deviation by thin dashed black curves. The corresponding predicted PSA/PGA ratios by the seismological model are shown by the solid red curve, and that of the empirical model of BA08 by the dashed blue curve.

0.06 s. Due to space limitations, only PSA/PGA plots for rock sites are shown. However, the results for both rock and soil sites show that the simulated PSA/PGA ratio curves are relatively insensitive to changes in $\Delta\sigma_L$ (and for that matter, any other model parameter), but are very sensitive to changes in κ. These plots confirm that the best overall fit is for $\kappa = 0.06$ s.

The longest distance bin in Figure 4.1, 150-300 km, shows a significant mismatch between observations and predictions that was not captured in the Sea99 plots of Figure 2.4. As the PSA/PGA

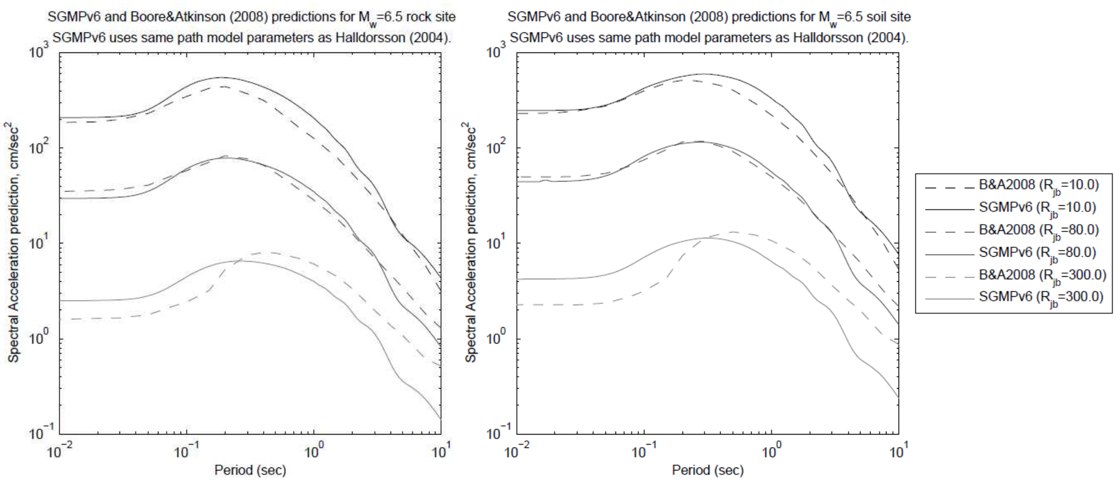

Figure 4.2. PSA predicted by BA08 compared with Fea12. Several path models were evaluated for better fits, but this remained the best and the prediction problems associated with long distances still remain. The plots are for rock (left) and soil (right) sites for $M_w = 6.5$.

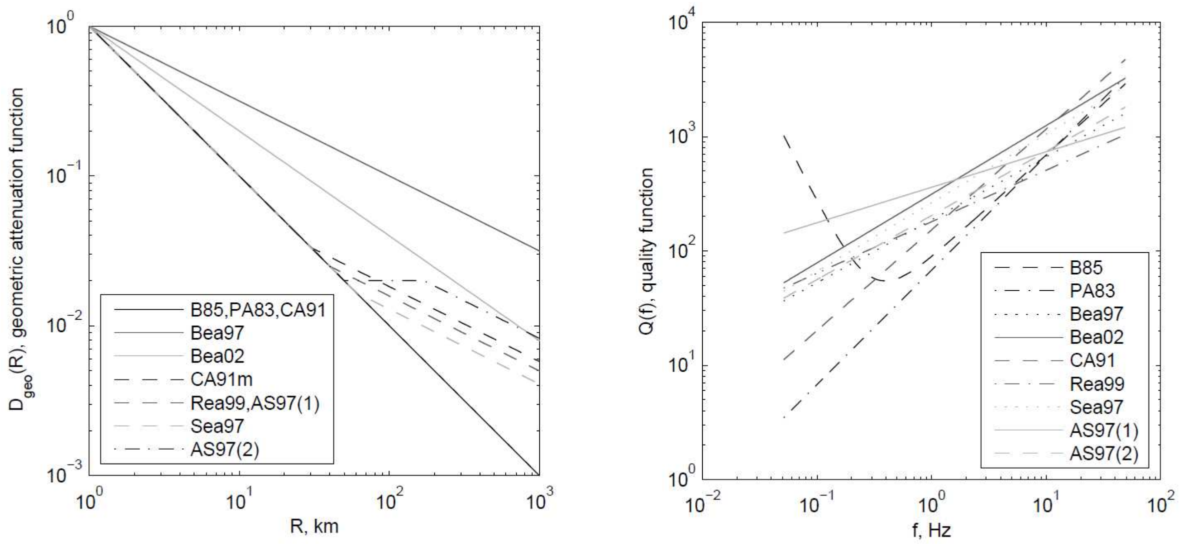

Figure 4.3. Different geometric spreading functions (left) and Q-functions (right) proposed by various researchers and evaluated by HP05 and Fea12.

plots are normalized, we refer to the individual residual plots for insight to the problem. The residual bins shown in Figure 2.2b indicate that our model tends to underpredict motions beyond about 15 0 km.

We concluded based on the above observations that model fit might be improved by modifying the path model: $P(f, r)$ in Equation (2.1). Up to now, our calibration had not questioned the assumptions of path or site terms in the model assembled by HP05. These were selected from a wide range of independent published path and site studies, so as to avoid inverting for multiple seismological model parameters which are prone to tradeoffs. We therefore re-examined these path models and evaluated their impact on the fit of the model. To evaluate the fits of these path functions efficiently, plots were generated in which the seismological model's PSA predictions, using one of the path models, were compared to BA08. Figure 4.2 shows an example. Several "best" model configurations were chosen based on visual evaluation of the fits of plots similar to those in Figure 4.1. These were then evaluated more thoroughly by the random-effects method. After examining the performance of all the models, the best model fit was still the one used by HP05. While near-source and mid-range predictions remain more important for most engineering applications, the problems of model performance at long distances discussed above still remained. Figure 4.3 shows all of the path models evaluated.

5. THE CHI-CHI AFTERSHOCK DATA

Finally we focus on the deteriorating fit of the seismological model to entire NGA dataset (a) as compared to dataset (c), both in terms of increasing bias at higher frequencies and increasing distance dependence at lower frequencies. This may indicate that the Chi-Chi data is inconsistent with the rest of the NGA dataset, which contains data mostly from shallow crustal earthquakes in interplate regions. The primary difference between the datasets is the Chi-Chi data, shown in Figure 5.1a. For half of the NGA dataset to consist of strong-motion data from a single region in itself causes the dataset to be biased. Although the random effects method accounts for such unbalanced datasets, the difference in model fits between datasets (c) and (a) is evident. The natural conclusion is therefore that the attenuation characteristics of strong-motion data (and possibly local stress drop) associated with the Chi-Chi main shock and aftershocks are not consistent with the rest of the NGA data. We investigated this by calculating the model bias and distance and magnitude dependencies of the residuals for the Chi-Chi data (mainshock with aftershocks, and only aftershocks). The results are shown in Figure 5.1b and confirm the above conclusion. We point out however, that the distance

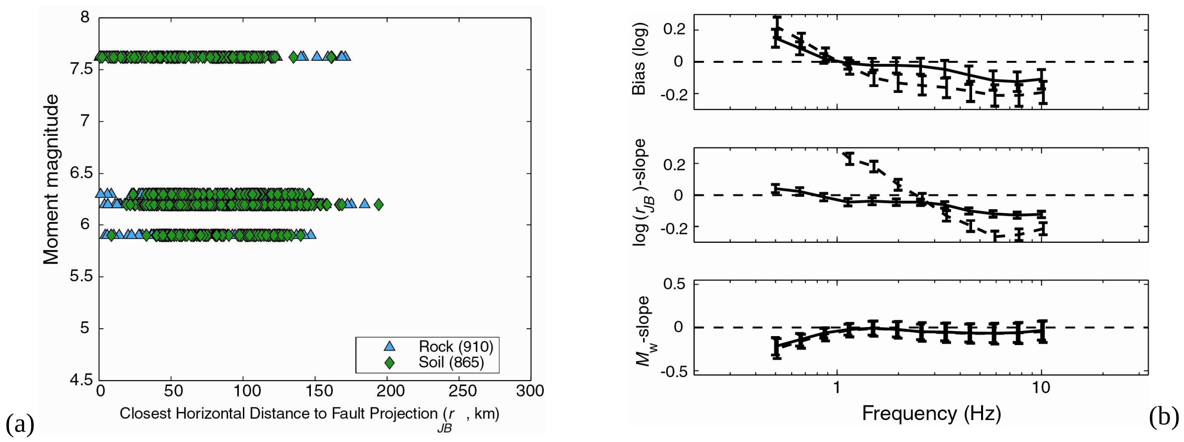

Figure 5.1. (a) Dataset consisting only of Chi-Chi data (compare with plots in Figure 2.1). (b) The concise plot of model fit to this data shows significant non-zero bias and distance dependences, for both rock and soil data. Note the relative differences between e.g., the fit shown in Figure 2.4c.

dependence (against $\log r_{JB}$) is quite evident in part because very few near-fault data exist (r_{JB} less than 1-2 fault dimensions) for the Chi-Chi earthquakes. Nevertheless, the disparity exists and we believe that a single path function (accounting for geometric spreading and anelastic attenuation of the types shown in Figure 4.3) as applied in our seismological model cannot remove it.

6. CONCLUSIONS

Trade-offs between parameters controlling the source, path and site effects in empirical models are unavoidable. For insight into the physical nature of such trade-offs a physical model is required. The one applied in this study fits the data relatively well. The Sea99 formalism and the PSA/PGA method are especially well suited to examining model performance in a physical context. We conclude that an improved path function is required to improve seismological model performance, especially at large distances. The disparity between the model fit to the (presumably more consistent) dataset (c) and the entire NGA dataset (a), which lies primarily with the Chi Chi strong-motion data, implies that the Chi-Chi data may be inconsistent with those comprising the rest of the dataset of strong-motion from shallow crustal earthquakes in interplate regions.

ACKNOWLEDGEMENT

This study was supported by the Leifur Eiriksson Foundation Scholarship Program (www.leifureirikssonfoundation.org) for Kevin M. Foster, and carried out at the Earthquake Engineering Research Centre (EERC) of the University of Iceland, in Selfoss, Iceland (www.eerc.hi.is), which also provided material support. Additional support was provided by the Icelandic Centre for Research (RANNIS) Project Grant No. 90049022. This support is gratefully acknowledged. We are additionally grateful to John Douglas, during his stay as Visiting Professor at the EERC, for fruitful discussions, including suggesting inspecting the PSA/PGA-behavior of model predictions vs. data. We are grateful for Dave Boore for pointing out an error in the caption of Figure 2 of Fea12 regarding the parameter ζ. It should be dimensionless and it takes values according to $\log\zeta = 2s_m(M_w - 6.35)$, where $s_m = -0.12$. Finally, $\kappa = 0.05$ s in Figure 2 of Fea12.

REFERENCES

Abrahamson, N.A. & Youngs, R.R. (1992) A stable algorithm for regression analyses using the random effects model. *Bulletin of the Seismological Society of America*, **82**, 505–510.

Aki, K. & Papageorgiou, A.S. (1988) Separation of source and site effects in acceleration power spectra of major California earthquakes. *Proc. 9th World Conf. Earthq. Eng* pp. 163–165.

Boore, D.M. (1983) Stochastic simulation of high-frequency ground motions based on seismological models of the radiated spectra. *Bulletin of the Seismological Society of America*, **73**, 1865–1894.

Boore, D.M. (2003) Simulation of Ground Motion Using the Stochastic Method. *Pure and Applied Geophysics*, **160**, 635–676.

Boore, D.M. & Atkinson, G.M. (2008) Ground-motion prediction equations for the average horizontal component of PGA, PGV, and 5%-damped PSA at spectral periods between 0.01 s and 10.0 s. *Earthquake Spectra*, **24**, 99.

Brillinger, D.R. & Preisler, H.K. (1984) An exploratory analysis of the Joyner-Boore attenuation data. *Bulletin of the Seismological Society of America*, **74**, 1441–1450.

Brillinger, D.R. & Preisler, H.K. (1985) Further analysis of the Joyner-Boore attenuation data. *Bulletin of the Seismological Society of America*, **75**, 611–614.

Chiou, B.S.-J., Darragh, R., Gregor, N. & Silva, W.J. (2008) NGA Project Strong-Motion Database. *Earthquake Spectra*, **24**, 23–44.

Foster, K.M., Halldorsson, B., Green, R.A. & Chapman, M.C. (2012) Calibration of the Specific Barrier Model to the NGA Dataset. *Seismological Research Letters*, **83**, 566–574.

Halldorsson, B., Mavroeidis, G.P. & Papageorgiou, A.S. (2011) Near-Fault and Far-Field Strong Ground Motion Simulation for Earthquake Engineering Applications Using the Specific Barrier Model. *Journal of Structural Engineering*, **137**, 433–444.

Halldorsson, B., Ólafsson, S. & Sigbjörnsson, R. (2007) A Fast and Efficient Simulation of the Far-Fault and Near-Fault Earthquake Ground Motions Associated with the June 17 and 21, 2000, Earthquakes in South Iceland. *Journal of Earthquake Engineering*, **11**, 343.

Halldorsson, B. & Papageorgiou, A.S. (2005) Calibration of the Specific Barrier Model to Earthquakes of Different Tectonic Regions. *Bulletin of the Seismological Society of America*, **95**, 1276–1300.

Halldorsson, B. & Papageorgiou, A.S. (2012a) Variations of the specific barrier model - Part I: Effect of subevent size distributions. *Bulletin of Earthquake Engineering*, Doi: 10.1007/s10518–012–9344–0.

Halldorsson, B. & Papageorgiou, A.S. (2012b) Variations of the specific barrier model - Part II: Effect of isochron distributions. *Bulletin of Earthquake Engineering*, Doi: 10.1007/s10518–012–9345–z.

Joyner, W.B. & Boore, D.M. (1986) On Simulating Large Earthquakes by Green’s Function Addition of Smaller Earthquakes. *Earthquake Source Mechanics* Maurice Ewing Series. (ed S. Das), pp. 269–274. American Geophysical Union.

Papageorgiou, A.S. (1988) On two characteristic frequencies of acceleration spectra: Patch corner frequency and f_{max}. *Bulletin of the Seismological Society of America*, **78**, 509–529.

Papageorgiou, A.S. (2003) The Barrier Model and Strong Ground Motion. *Pure and Applied Geophysics*, **160**, 603–634.

Papageorgiou, A.S. & Aki, K. (1983a) A specific barrier model for the quantitative description of inhomogeneous faulting and the prediction of strong ground motion. I. Description of the model. *Bulletin of the Seismological Society of America*, **73**, 693–722.

Papageorgiou, A.S. & Aki, K. (1983b) A specific barrier model for the quantitative description of inhomogeneous faulting and the prediction of strong ground motion. Part II. Applications of the model. *Bulletin of the Seismological Society of America*, **73**, 953–978.

Papageorgiou, A.S. & Aki, K. (1985) Scaling law of far-field spectra based on observed parameters of the specific barrier model. *Pure and Applied Geophysics*, **123**, 353–374.

Power, M., Chiou, B.S.-J., Abrahamson, N.A., Bozorgnia, Y., Shantz, T. & Roblee, C. (2008) An Overview of the NGA Project. *Earthquake Spectra*, **24**, 3–21.

Spudich, P., Joyner, W.B., Lindh, A.G., Boore, D.M., Margaris, B.M. & Fletcher, J.B. (1999) SEA99: A revised ground motion prediction relation for use in extensional tectonic regimes. *Bulletin of the Seismological Society of America*, **89**, 1156–1170.

Strasser, F.O., Abrahamson, N.A. & Bommer, J.J. (2009) Sigma: Issues, Insights, and Challenges. *Seismological Research Letters*, **80**, 40–56.